Rapid Communications

Multiscale control of active emulsion dynamics

Livio Nicola Carenza,[1,*] Luca Biferale,[2] and Giuseppe Gonnella[1]
[1]*Dipartimento di Fisica, Università degli Studi di Bari and INFN, Sezione di Bari, Bari, I-70126, Italy*
[2]*Dipartimento di Fisica and INFN, Università di Roma "Tor Vergata," 00133 Roma, Italy*

(Received 10 June 2019; published 16 January 2020)

We numerically study the energy transfer in a multicomponent two-dimensional film made of an active polar gel and a passive isotropic fluid in presence of surfactant favoring emulsification. We show that by confining the active behavior into the localized component, the typical scale where chemical energy is transformed in mechanical energy can be substantially controlled. Quantitative analysis of kinetic energy spectra and fluxes shows the presence of a multiscale dynamics due to the existence of a flux induced by the active stress only, without the presence of a turbulent cascade. An increase in the intensity of active doping induces drag reduction due to the competition of elastic and dissipative stresses against active forces. Furthermore we show that a nonhomogeneous activity pattern induces localized response, including a modulation of the slip length, opening the way toward the control of active flows by external variation of the actvity level.

DOI: 10.1103/PhysRevFluids.5.011302

I. INTRODUCTION

Active fluids exhibit a number of peculiar behaviors due to the small-scale conversion of internal into mechanical energy by the active constituents. Many biological examples, such as bacterial [1,2] and cytoskeletal suspensions [3–5] and artificial systems, e.g., Janus [6,7] and magnetic microparticles [8], have been studied in the labs and by numerical simulations. In the presence of high concentration of the active component, there exists the possibility to develop complex (chaotic) flows even in the absence of any external forcing, due to active injection only [9–11]. This is a nontrivial collective phenomenon [12], also leading to rich rheological properties, including cases of vanishing and negative effective viscosity [13–16] or preferential clustering [17–20].

Understanding the dense-suspension limit is pivotal to develop novel fluid materials with *ad hoc* and controllable space-time dependent features, a challenge for both fundamental and applied (micro) fluid mechanics. Recently, very interesting results have been produced, pointing toward the possibility to develop fluid motion at mesoscales, i.e., at distances much larger than the typical single-agent size and with a kinetic energy spectrum characterized by power-law behavior in a limited range of scales. The term *bacterial turbulence* has been coined for that [1,10,21–24], with a puzzling variety of nonuniversal behaviors [1,8,21,24–26].

In this Rapid Communication, we want to quantitatively disentangle the different mechanisms behind the development of complex active flows for the important case of a composite fluid: a two-dimensional (2D) active polar gel in a passive isotropic fluid matrix [27,28]. Differt from most of the previous studies, we are interested in the set-up where the active matter is confined in a dropletlike emulsion phase (see Fig. 1), whose experimental realization can be achieved, e.g., by confining cellular extracts in a water-in-oil emulsion [3,4] or in bacterial systems subjected to

*Corresponding author: livio.carenza@ba.infn.it

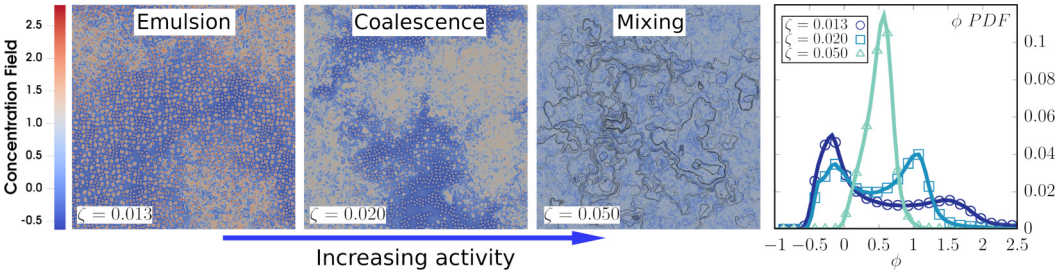

FIG. 1. Contour plot of concentration field ϕ, where the active component is red and the passive one is blue showing late-time configurations of active fluids at different intensities of active doping ζ. Velocity streamlines are plotted in black for the case at $\zeta = 0.050$. Last panel: *pdf* of the concentration field; notice the transition to mixing for $\zeta > 0.020$ characterized by the presence of a single peak.

depletion forces leading to microphase separation [29]. Our set-up is particularly appealing because it allows us to change the degree of localization of the energy injection by the active matter—which is a way to control forcing mechanisms in real flows. By moving from a confined emulsion to a phase with large aggregates of active material and then to a fully dispersed (mixed) regime, we are able to systematically address the relevant scales of the active component for the chaotic flow evolution (see Fig. 1). We clarify the difference between an *active turbulent* and an *active elastic* flow and we argue that active gels cannot exhibit a turbulent nonlinear cascade, as the velocity field is driven by the active field only. We discuss the key observable that must be controlled in order to distinguish and classify the flow properties, stressing that the energy spectrum is not informative enough and cannot be used to distinguish between the presence of an inverse/direct cascade or even no cascade at all [30]. Concerning more applied aspects, we show that a suitable space-time modulation of the doping is capable to fine-tune the flow response and the mixture morphology, opening the unexplored direction for active-control of (micro) active fluids.

II. THE MODEL

The orientable nature of many active constituents has been successfully modeled by means of the Landau-De Gennes theory for liquid crystals, introducing a coarse-grained *polarization field* $\mathbf{P}$, accounting for the local orientation of constituents, while the local *concentration* of active material is described by the conserved field ϕ. The evolution of the system is governed by the following equations, in the limit of incompressible flow:

$$\begin{aligned} &\rho(\partial_t + \mathbf{v}\cdot\nabla)\mathbf{v} = \nabla\cdot(\tilde{\sigma}^{\text{pass}} + \tilde{\sigma}^{\text{act}}),\\ &\partial_t\phi + \nabla\cdot(\phi\mathbf{v}) = M\nabla^2\mu,\\ &\partial_t\mathbf{P} + (\mathbf{v}\cdot\nabla)\mathbf{P} = -\tilde{\Omega}\cdot\mathbf{P} + \xi\tilde{D}\cdot\mathbf{P} - \frac{\mathbf{h}}{\Gamma}. \end{aligned} \tag{1}$$

Here the first equation is the incompressible Navier-Stokes equation [31], where $\mathbf{v}$ is the velocity field and ρ the total (constant) density, while the stress tensor has been divided in a passive term,

$$\tilde{\sigma}^{\text{pass}} = \tilde{\sigma}^{\text{hydro}} + \tilde{\sigma}^{\text{bin}} + \tilde{\sigma}^{\text{pol}},$$

given by the conserved momentum current, including viscous and ideal fluid pressure contributions [32], and a phenomenological traceless active term [33,34],

$$\tilde{\sigma}^{\text{act}} = -\zeta\phi\left(\mathbf{P}\otimes\mathbf{P} - \frac{\mathbf{I}}{2}\mathbf{P}^2\right).$$

The *activity* parameter ζ tunes the intensity of active doping: If positive, then it describes the stress exerted by pusher swimmers—thus generating *extensile* quadrupolar flow patterns [34]. Pullers can be modeled with negative values of ζ. In this Rapid Communication, we will restrict our study to $\zeta > 0$, since most biological extracts exhibiting complex behaviors are pushers. The second equation rules the convection-diffusion evolution of active concentration ϕ. Here M is the mobility, while the chemical potential $\mu = \delta\mathcal{F}/\delta\phi$ is derived from a phenomenological model—a generalization of the Brazovskii free energy [27,28,35,36]:

$$\mathcal{F}[\phi, \mathbf{P}] = \int \left[\frac{a}{4\phi_{\rm cr}^2}\phi^2(\phi-\phi_0)^2 + \frac{k_\phi}{2}(\nabla\phi)^2 + \frac{c}{4}(\nabla^2\phi)^2 - \frac{\alpha}{2}\frac{(\phi-\phi_{\rm cr})}{\phi_{\rm cr}}\mathbf{P}^2 + \frac{\alpha}{4}\mathbf{P}^4 + \frac{k_P}{2}(\nabla\mathbf{P})^2 + \beta\mathbf{P}\cdot\nabla\phi \right] d\mathbf{r}. \tag{2}$$

Phase separation of the two components is obtained with bulk energy density $a > 0$ to have two minima in the free-energy at $\phi = 0, \phi_0$. By choosing $k_\phi < 0$, interface formation is favored, so that the Brazovskii constant c must be positive to guarantee thermodynamic stability. Setting $\alpha > 0$, the polarization field $\mathbf{P}$ is confined in the *active* regions (where $\phi > \phi_{\rm cr} = \phi_0/2$) and is absent in *passive* regions, where $\phi < \phi_{\rm cr}$. The energy cost for the elastic deformations is paid by the gradient term $(\nabla\mathbf{P})^2$ [37]. Homeotropic anchoring is obtained by setting $\beta > 0$ [38]. This is done to replicate the behavior of some experimental systems where the mean orientation of the constituents is normal to interfaces [39,40].

In the passive limit ($\zeta = 0$) and for asymmetric compositions ($\overline{\phi/\phi_0} \lesssim 0.35$, with the bar denoting spacial average) the system sets into an array of droplets of the minority phase in an isotropic background [16], see also Fig. 1. Finally, the evolution of the polarization field is governed by the Ericksen-Leslie equation for a vector order parameter [41]. Here $\mathbf{h} = \delta\mathcal{F}/\delta\mathbf{P}$ is the molecular field and Γ the rotational viscosity, while the symmetric deformation rate tensor is $\tilde{D} = \frac{1}{2}(\nabla\mathbf{v} + \nabla\mathbf{v}^T)$ and the vorticity tensor is $\tilde{\Omega} = \frac{1}{2}(\nabla\mathbf{v} - \nabla\mathbf{v}^T)$; we choose the shape factor $\xi > 1$ to model flow-aligning rodlike swimmers [27,28]. In Fig. 1 we show for the first time the existence of a transition to a final mixed phase by increasing the activity ζ. This is due to the fact that strengthening the doping induces more and more active stress across the droplets, leading to interface breaking and droplet coalescence. The consecutive dispersion of active agents in the whole volume has the important effect of changing the typical flow length scales since small-scale deformation of the polarization pattern is wiped out. Similarly, a decrease in the viscosity η makes more efficient the active pumping in the flow, leading to the same conclusion. It is important to stress that the nature of the transition is not known. As far as our numerical studies suggest, it is probably continuous but a much more detailed investigation is needed to clarify this point, which is not the main goal of this paper. In what follows, we will investigate the kinematic and flow properties at changing ζ.

III. NUMERICAL RESULTS

We performed a systematic series of numerical simulations by fixing all free parameters in Eqs. (1) and (2) to values that correspond to a realistic description of active cytoskeletal suspensions [3,42,43]—an experimental system that is known to exhibit a chaotic flow dynamics even at small Re [3,4] (see Table I for the mapping between physical and simulation units and SM for the Reynolds number measured from simulations [32]). We systematically changed the intensity of the active doping ζ, integrating Eqs. (1) by means of a widely validated hybrid lattice Boltzmann (LB) approach [44,45], on a squared periodical 2D lattice of size $L = 1024$, except otherwise stated. In Fig. 2 we start by showing the energy spectra per unit density $E(k) = 0.5\langle|\mathbf{v}(\mathbf{k})|^2\rangle$, where $\langle\cdot\rangle$ stands for the steady-state spherical average for different values of ζ (left panel). Remarkably, we found the presence of a continuum spectrum even for wave numbers smaller than the typical injection scale k_a, where the active matter is preferentially confined. The spectral properties depend

TABLE I. Mapping between physical and simulation units. Length scale $l^* = 1$ μm, timescale $t^* = 10$ ms, and force scale $f^* = 10^2$ nN are set to 1 in LB units. Viscosity η is expressed in kPa s, the elastic constant of the polar gel k_P in nN, the diffusivity $D = \mathrm{Ma}$ in $\mu\mathrm{m}^2\,\mathrm{s}^{-1}$, while Γ and ζ are respectively expressed in kPa s and kPa.

Units	η	k_P	D	Γ	ζ
Simulation	5/6	0.01	0.0004	1	0.01–0.06
Physical	0.83	10	0.004	10	100–600

on the activity ζ, with an accumulation of energy at scales larger than k_v as soon as the coalescence starts to act. The typical Reynolds numbers are $\mathrm{Re} \sim 10^{-2}$ to 1, a regime close to experimental observations, where we defined $\mathrm{Re} = \rho E^{1/2}(k_v) l_v/\eta$ in terms of the typical flow wave number $k_v = [\int_0^\infty dk' k' E(k')]/E_{\mathrm{tot}}$—namely the first moment of the energy distribution—and length scale $l_v = L/k_v$, where $E_{\mathrm{tot}} = \int_0^\infty dk' E(k')$ is the total kinetic energy. The right panel of the same figure shows the spectral properties of the active energy injection:

$$\mathcal{S}^{\mathrm{act}}(k,t) = \langle \mathbf{v}^*(\mathbf{k},t) \cdot \mathbf{F}^{\mathrm{act}}(\mathbf{k},t) \rangle, \tag{3}$$

where $\mathbf{F}^{\mathrm{act}}(k,t) = 2\pi i \mathbf{k} \cdot \tilde{\sigma}^{\mathrm{act}}(\mathbf{k},t)/L$. As anticipated, energy pumping is considerably localized at high wave number ($k_a/L = l_a^{-1} \simeq 0.1$, being k_a the first moment of $\mathcal{S}^{\mathrm{act}}$) when activity is low enough, due to small-scale deformations of the polarization field homeotropically and strongly anchored to interfaces [27,28]. By increasing ζ, as the system undergoes first coalescence ($\zeta = 0.02$) and then mixing, interfaces broaden and progressively disappear, thus attenuating energy supply at high wave numbers and leading to a situation where energy is injected on a wider range of scales, typical of the active-driven bending instabilities of the polar gel [12,46].

Going back to the spectra, we notice that the presence of small droplets of typical size $l_d = L/k_d \simeq 15$ does not produce any Gibbs effects: As long as the droplet phase survives, energy is accumulated on the typical length scale of the droplet size as suggested by the bulge in energy spectra, for small values of ζ, located at wave number k_d. As confinement is lost ($\zeta \gtrsim 0.035$), energy is instead spread on much larger scales ($k_v/L = l_v^{-1} \simeq 0.025$). Even more interesting is the observation that the energy injected in the system at low activity is substantially greater than the one delivered at higher active dopings.

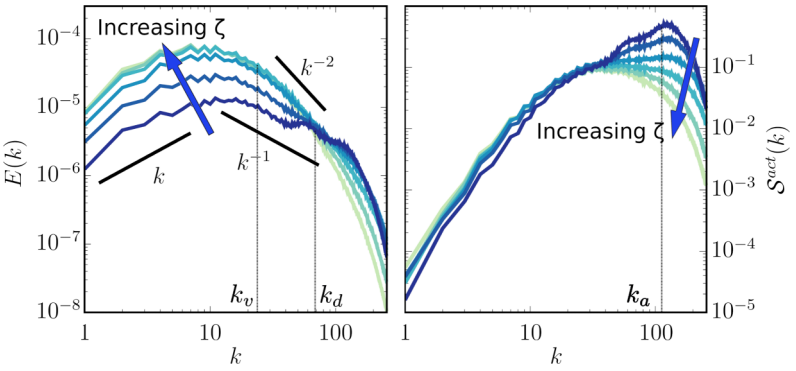

FIG. 2. Left: Log-log plot of time-averaged energy spectra varying activity ($\zeta = 0.013, 0.015, 0.02, 0.03, 0.04, 0.05$). Right: Total amount of energy injected in the system by active agents. Vertical black dashed lines mark the wave number k_v, k_d, and k_a, respectively (see text), for the case at $\zeta = 0.05$.

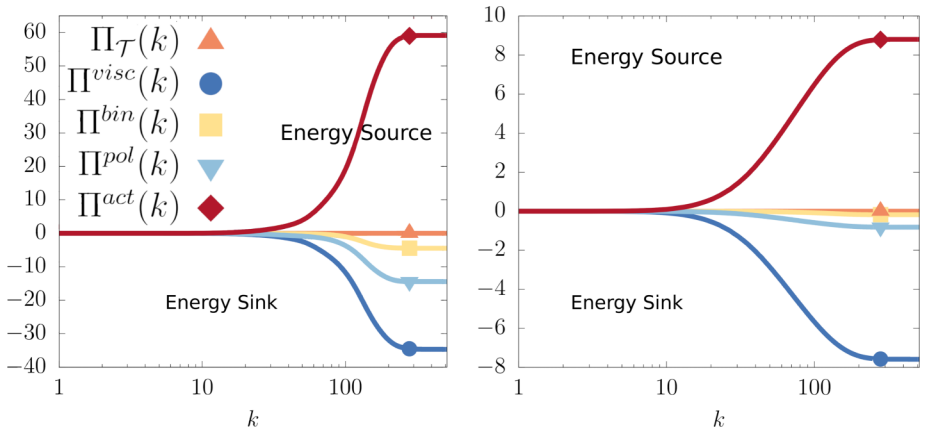

FIG. 3. Time-averaged components of the total energy flux at $\zeta = 0.013$ (left) and $\zeta = 0.050$ (right). Notice the different y range in the two graphs.

This surprising behavior (and its connection to morphology) has been confirmed by keeping fixed the active parameter $\zeta = 0.015$ and varying the nominal viscosity of the suspension (not shown). Once again we found that total kinetic energy rises and develops on progressively bigger length scales as viscous effects are lowered and mixing of the two components occurs, thus driving the active agents in an unconfined state.

It is well known that spectra do not bring enough information to disentangle the complicated network of transfer mechanisms inside a complex flow [30]. Thus, we performed a systematic analysis of the energy balance in Fourier space by looking at the scale-by-scale contribution of all terms, either dissipative or reactive. We thus Fourier transform both sides of the Navier-Stokes equation and we multiply them by $\mathbf{v}^*(\mathbf{k})$ to obtain the following balance equation, spherically averaged on shells of equal momentum:

$$\rho \partial_t E(k,t) + \mathcal{T}(k,t) = \sum_i \mathcal{S}^{(i)}(k,t). \tag{4}$$

Here $\mathcal{T}(k,t) = \langle \mathbf{v}^*(\mathbf{k},t) \cdot \mathbf{J}(\mathbf{k},t) \rangle$ represents the rate of energy transfer due to nonlinear hydrodynamic interactions [with $\mathbf{J}(\mathbf{k},t)$ standing for the Fourier transform of $\rho \mathbf{v} \cdot \nabla \mathbf{v} + \nabla p$]. The terms on the right-hand side of Eq. (4) are energy source/sink contributions, where the terms $\mathcal{S}^{(i)}(k,t)$ are defined as in Eq. (3) and (i) denotes the different kinds of contributions: viscous, binary, polar, or active (see SM for explicit definition [32]). Finally, we define each separate component of the energy flux as the total variation per unit time of the energy contained in a sphere of radius k:

$$\Pi^{(i)}(k) = \int_0^k dk' \mathcal{S}^{(i)}(k'), \quad \Pi_{\mathcal{T}}(k) = \int_0^k dk' \mathcal{T}(k').$$

Figure 3 shows fluxes for $\zeta = 0.013, 0.050$, measured at steady state. In both cases, the only source contribution is the active one, Π^{act}, while all the others are energy sinks. Before the transition to mixing [$\zeta = 0.013$, Fig. 3 (left)] the binary and polar terms are also contributing (as sinks). After, the dynamics is characterized by an almost perfect matching among viscous and active terms [Fig. 3 (right)]. The advection term, $\Pi_{\mathcal{T}}$, is, for all practical effects, null, as expected for fluids flowing at negligible Reynolds numbers. The previous findings suggest some important conclusions. First, the scenario is in agreement with *the absence* of hydrodynamic turbulence. Here multiscale effects and chaotic evolution arise from the competition between sink terms and active injection, leading to a nontrivial scale-to-scale balance. The phenomenology is similar to the case of *elastic turbulence*, where the nonlinear evolution for the velocity field is dominated by the non-Newtonian stress,

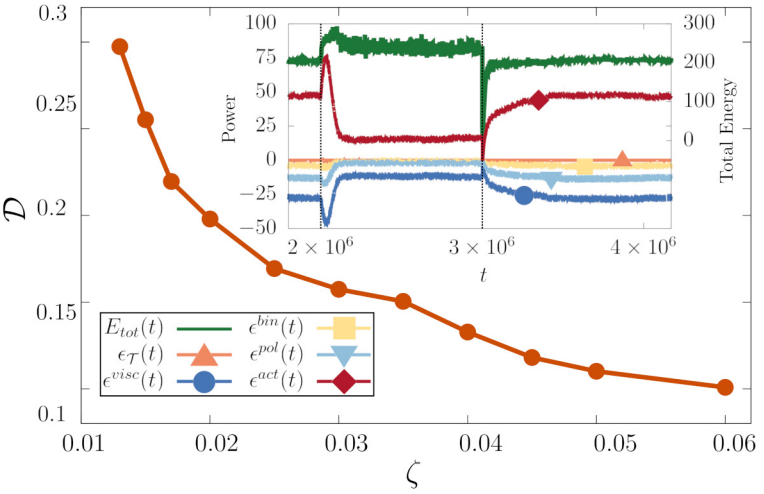

FIG. 4. Drag factor versus activity. Inset shows time evolution of kinetic energy $E_{\rm tot}$ and power terms $\epsilon^{(i)}(t)$ defined in the same way as $\epsilon^{\rm act}(t)$, while rising activity from $\zeta = 0.010$ to $\zeta = 0.030$ at time t_1 and reducing it to its previous value at time t_2, denoted by vertical dashed lines.

leading to chaotic and unpredictable multiscale evolution even at nominally vanishing Reynolds numbers [47–49]. Second, the overwhelming role played by the active stress explains the absence of universality [1,8,21] in many biofluids: There is no direct or inverse energy cascade mediated by the universal advection flux, $\Pi_{\mathcal{T}}$. Energy is moved from scale to scale by the direct interaction with the case-specific active stress. The absence of a turbulent cascade is one of the main results of our paper. Moreover, we observe that we only draw conclusions based on observations of the fluxes behavior in the high-k region, where the system is translationally invariant and fluxes are significantly non-null (see Fig. 3), regardless of the intensity of the activity parameter. In this region the spectral analysis is not affected by phase-separation effects (which may become important at smaller wave numbers in the coalescence phase) since the typical length scale of domains—comparable with the size of the simulation box—is considerably larger than the typical flow length scale.

To quantitatively characterize the efficiency of injection of energy pumped in the system by active effects, we define the *drag factor*:

$$\mathcal{D} = \frac{\epsilon^{\rm act} l_v}{E_{\rm tot}^{3/2}}$$

in terms of the total energy injected by active forces, the only source contribution $\epsilon^{\rm act} = \lim_{k\to\infty} \Pi^{\rm act}(k)$, the total response, given by the available kinetic energy $E_{\rm tot}$, and l_v. In Fig. 4 we show the results for $\mathcal{D}$ at varying the activity ζ. We note that the drag factor rapidly decreases while increasing activity in the emulsion phase and then the decrease slows down as big active clusters become dominant in the system and finally tends to saturation when the morphological transition toward mixing takes place. Drag reduction is a further evidence of the shear thinning behavior exhibited by extensile suspensions [50,51].

IV. SPACE-TIME CONTROL

Finally, to test the dynamical response of active emulsions we performed a numerical study when we abruptly rise ζ across the mixing transition from 0.013 to $\zeta = 0.030$. Kinetic energy rapidly increases in a short transient and finally sets to a new stable value higher than before. Power terms behavior is instead characterized by a spike in correspondence of the transient, followed

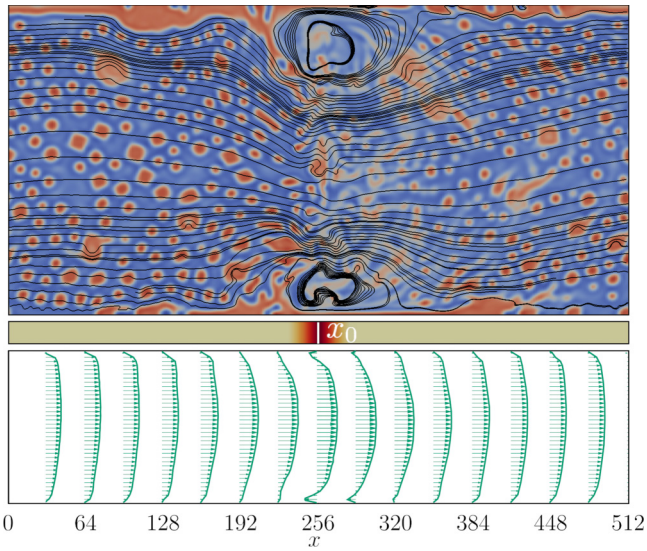

FIG. 5. Contour plot of concentration of active and passive phases in an externally controlled active emulsion subject to Poiseuille flow in a 512×256 channel (color legend is the same as in Fig. 1). Velocity streamlines are plotted in black, showing effective reduction of the channel width. Activity ζ is modulated in the flow direction as shown in the central color bar [beige corresponds to $\zeta = 0.010$, while $\zeta(x_0) = 0.03$]. Time-averaged profiles of v_x are shown in the last panel. Notice that profiles close to x_0 exhibit a non-null (negative) slip length.

by relaxation toward much smaller values. This behavior is found to be reversible, without the appearence of any hysteresis feature that may eventually occur in unconfined active gels [13,50]: Indeed, when activity is lowered again kinetic energy rapidly restore its previous values, as well as power terms (see inset of Fig. 4). Finally, in Fig. 5 we show a space-dependent protocol to control the flow response. We studied the evolution of the active polar gel emulsion on a channel under constant pressure gradient and by changing the activity parameter as a function of the position downstream $\zeta(x)$. In particular we show that a local sharp increase of ζ above the mixing transition around $x \sim x_0$ is a tool to locally control the degree of emulsification in the bulk, opening the way to change the flow transport properties and the flow topology *on-the-fly* [52,53].

V. CONCLUSIONS

By using systematic numerical investigation of a 2D active emulsion we have shown that a nontrivial multiscale chaotic dynamics develops due to the direct injection of chemical/internal energy into the flow evolution. We showed that the relative effects of advection, viscous, reactive forces do change when varying the activity of the dispersed phase. In particular, for low activity, the flow structures are driven by the active stress and dissipated by the polar and viscous components mainly. For large activity, the flow undergoes a morphological transition, with the two fluids (active and passive) both well mixed and active forces are balanced by the viscous drag only. This must be considered a first hint that active emulsions are able to develop flow configurations with a wide range of dynamical scales. An increase in the intensity of active doping induces drag reduction due to the competition of elastic and dissipative stresses against active forces. Furthermore, we have shown that a nonhomogeneous pattern of activity in the bulk induces a localized response opening the way toward the control of active flows by modulated activity.

ACKNOWLEDGMENTS

Simulations were ran at Bari ReCaS e-Infrastructure funded by MIUR through PON Research and Competitiveness 2007-2013 Call 254 Action I.

[1] H. H. Wensink, J. Dunkel, S. Heidenreich, K. Drescher, H. Lowen, R. E. Goldstein, and J. M. Yeomans, Meso-scale turbulence in living fluids, Proc. Natl. Acad. Sci. USA **109**, 14308 (2012).
[2] J. Dunkel, S. Heidenreich, K. Drescher, H. H. Wensink, M. Bär, and R. E. Goldstein, Fluid Dynamics of Bacterial Turbulence, Phys. Rev. Lett. **110**, 228102 (2013).
[3] T. Sanchez, D. T. N. Chen, S. J. Decamp, M. Heymann, and Z. Dogic, Spontaneous motion in hierarchically assembled active matter, Nature **491**, 431 (2012).
[4] P. Guillamat, J. Ignés-Mullol, and F. Sagués, Control of active liquid crystals with a magnetic field, Proc. Natl. Acad. Sci. USA **113**, 5498 (2016).
[5] P. Guillamat, Z. Kos, J. Hardoüin, M. Ravnik, and R. Sagués, Active nematic emulsions, Sci. Adv. **4**, eaao1470 (2018).
[6] S. Ebbens, D. A. Gregory, G. Dunderdale, J. R. Howse, Y. Ibrahim, T. B. Liverpool, and R. Golestanian, Electrokinetic effects in catalytic platinum-insulator janus swimmers, Europhys. Lett. **106**, 58003 (2014).
[7] D. A. Gregory, A. I. Campbell, and S. J. Ebbens, The effect of catalyst distribution on spherical bubble swimmer trajectories, J. Phys. Chem. C **119**, 15339 (2015).
[8] G. Kokot, S. Das, R. G. Winkler, G. Gompper, I. S. Aranson, and A. Snezhko, Active turbulence in a gas of self-assembled spinners, Proc. Natl. Acad. Sci. USA **114**, 12870 (2017).
[9] M. C. Marchetti, J. F. Joanny, S. Ramaswamy, T. B. Liverpool, J. J. Prost, M. Rao, and R. A. Simha, Hydrodynamics of soft active matter, Rev. Mod. Phys. **85**, 1143 (2013).
[10] A. Doostmohammadi, T. N. Shendruk, K. Thijssen, and J. M. Yeomans, Onset of meso-scale turbulence in active nematics, Nat. Commun. **8**, 15326 (2017).
[11] L. N. Carenza, G. Gonnella, A. Lamura, G. Negro, and A. Tiribocchi, Lattice boltzmann methods and active fluids, Eur. Phys. J. E **42**, 81 (2019).
[12] R. Voituriez, J. F. Joanny, and J. Prost, Spontaneous flow transition in active polar gels, Eurphys. Lett. **70**, 404 (2005).
[13] M. E. Cates, S. M. Fielding, D. Marenduzzo, E. Orlandini, and J. M. Yeomans, Shearing Active Gels Close to the Isotropic-Nematic Transition, Phys. Rev. Lett. **101**, 068102 (2008).
[14] H. M. López, J. Gachelin, C. Douarche, H. Auradou, and E. Clément, Turning Bacteria Suspensions into Superfluids, Phys. Rev. Lett. **115**, 028301 (2015).
[15] A. Loisy, J. Eggers, and T. B. Liverpool, Active Suspensions have Nonmonotonic Flow Curves and Multiple Mechanical Equilibria, Phys. Rev. Lett. **121**, 018001 (2018).
[16] G. Negro, L. N. Carenza, A. Lamura, A. Tiribocchi, and G. Gonnella, Rheology of active polar emulsions: From linear to unidirectional and unviscid flow, and intermittent viscosity, Soft Matter **15**, 8251 (2019).
[17] Y. Fily and M. C. Marchetti, Athermal Phase Separation of Self-Propelled Particles with No Alignment, Phys. Rev. Lett. **108**, 235702 (2012).
[18] I. Buttinoni, J. Bialké, F. Kümmel, H. Löwen, C. Bechinger, and T. Speck, Dynamical Clustering and Phase Separation in Suspensions of Self-Propelled Colloidal Particles, Phys. Rev. Lett. **110**, 238301 (2013).
[19] P. Digregorio, D. Levis, A. Suma, L. F. Cugliandolo, G. Gonnella, and I. Pagonabarraga, Full Phase Diagram of Active Brownian Disks: From Melting to Motility-Induced Phase Separation, Phys. Rev. Lett. **121**, 098003 (2018).
[20] L. F. Cugliandolo, P. Digregorio, G. Gonnella, and A. Suma, Phase Coexistence in Two-Dimensional Passive and Active Dumbbell Systems, Phys. Rev. Lett. **119**, 268002 (2017).
[21] V. Bratanov, F. Jenko, and E. Frey, New class of turbulence in active fluids, Proc. Natl. Acad. Sci. USA **112**, 15048 (2015).

[22] C. Dombrowski, L. Cisneros, S. Chatkaew, R. E. Goldstein, and J. O. Kessler, Self-Concentration and Large-Scale Coherence in Bacterial Dynamics, Phys. Rev. Lett. **93**, 098103 (2004).
[23] T. N. Shendruk, A. Doostmohammadi, K. Thijssen, and J. M. Yeomans, Dancing disclinations in confined active nematics, Soft Matter **13**, 3853 (2017).
[24] L. Giomi, Geometry and Topology of Turbulence in Active Nematics, Phys. Rev. X **5**, 031003 (2015).
[25] A. Creppy, O. Praud, X. Druart, P. L. Kohnke, and F. Plouraboué, Turbulence of swarming sperm, Phys. Rev. E **92**, 032722 (2015).
[26] M. Linkmann, G. Boffetta, M. C. Marchetti, and B. Eckhardt, Phase Transition to Large Scale Coherent Structures in Two-Dimensional Active Matter Turbulence, Phys. Rev. Lett. **122**, 214503 (2019).
[27] F. Bonelli, L. N. Carenza, G. Gonnella, D. Marenduzzo, E. Orlandini, and A. Tiribocchi, Lamellar ordering, droplet formation and phase inversion in exotic active emulsions, Sci. Rep. **9**, 2801 (2019).
[28] G. Negro, L. N. Carenza, P. Digregorio, G. Gonnella, and A. Lamura, Morphology and flow patterns in highly asymmetric active emulsions, Physica A **503**, 464 (2018).
[29] J. Schwarz-Linek, C. Valeriani, A. Cacciuto, M. E. Cates, D. Marenduzzo, A. N. Morozov, and W. C. K. Poon, Phase separation and rotor self-assembly in active particle suspensions, Proc. Natl. Acad. Sci. USA **109**, 4052 (2012).
[30] A. Alexakis and L. Biferale, Cascades and transitions in turbulent flows, Phys. Rep. **767-769**, 1 (2018).
[31] L. D. Landau and E. M. Lifshitz, *Fluid Mechanics: Vol 6, volume 6 of Course of Theoretical Physics*, 2nd ed. (Butterworth-Heinemann Ltd, London, 1987).
[32] See Supplemental Material at http://link.aps.org/supplemental/10.1103/PhysRevFluids.5.011302 for further informations regarding the model, numerical method, and further validation of results.
[33] T. J. Pedley and J. O. Kessler, Hydrodynamic phenomena in suspensions of swimming microorganisms, Annu. Rev. Fluid Mech. **24**, 313 (1992).
[34] Y. Hatwalne, S. Ramaswamy, M. Rao, and R. A. Simha, Rheology of Active-Particle Suspensions, Phys. Rev. Lett. **92**, 118101 (2004).
[35] S. A. Brazovskiĭ, Phase transition of an isotropic system to a nonuniform state, J. Exp. Theor. Phys. **41**, 85 (1975).
[36] G. Gonnella, E. Orlandini, and J. M. Yeomans, Spinodal Decomposition to a Lamellar Phase: Effects of Hydrodynamic Flow, Phys. Rev. Lett. **78**, 1695 (1997).
[37] P. G. de Gennes and J. Prost, *The Physics of Liquid Crystals*, The International Series of Monographs on Physics, Vol. 83, 2nd ed. (Oxford University Press, Oxford, 1993).
[38] It is known that the sign of β is not affecting the stability of the droplet phase, since this depends only on β^2 [16].
[39] P. C. Mushenheim, R. R. Trivedi, S. S. Roy, M. S. Arnold, D. B. Weibel, and N. L. Abbott, Effects of confinement, surface-induced orientations and strain on dynamical behaviors of bacteria in thin liquid crystalline films, Soft Matter **11**, 6821 (2015).
[40] S. Zhou, O. Tovkach, D. Golovaty, A. Sokolov, I. S. Aranson, and O. D. Lavrentovich, Dynamic states of swimming bacteria in a nematic liquid crystal cell with homeotropic alignment, New J. Phys. **19**, 055006 (2017).
[41] A further self advecting term of the form $w\mathbf{P}\cdot\nabla\mathbf{P}$ may be included to the evolution equation for the polarization field, with $\mathbf{w}$ the swimming speed of the active constitutents. We set $w = 0$ that allows for the description of shakers namley organisms only capable to stress the surrounding fluid.
[42] E. Tjhung, D. Marenduzzo, and M. E. Cates, Spontaneous symmetry breaking in active droplets provides a generic route to motility, Proc. Natl. Acad. Sci. USA **109**, 12381 (2012).
[43] E. Tjhung, A. Tiribocchi, D. Marenduzzo, and M. E. Cates, A minimal physical model captures the shapes of crawling cells, Nat. Commun. **6**, 5420 (2015).
[44] S. Succi, *The Lattice Boltzmann Equation: For Fluid Dynamics and Beyond*, Numerical Mathematics and Scientific Computation (Clarendon Press, London, 2001).
[45] C. Denniston, E. Orlandini, and J. M. Yeomans, Lattice boltzmann simulations of liquid crystal hydrodynamics, Phys. Rev. E **63**, 056702 (2001).
[46] L. Giomi, M. C. Marchetti, and T. B Liverpool, Complex Spontaneous Flows and Concentration Banding in Active Polar Films, Phys. Rev. Lett. **101**, 198101 (2008).

[47] R. G. Larson, Fluid dynamics: Turbulence without inertia, Nature **405**, 27 (2000).
[48] T. Burghelea, E. Segre, and V. Steinberg, Role of Elastic Stress in Statistical and Scaling Properties of Elastic Turbulence, Phys. Rev. Lett. **96**, 214502 (2006).
[49] A. N. Morozov and W. van Saarloos, An introductory essay on subcritical instabilities and the transition to turbulence in visco-elastic parallel shear flows, Phys. Rep. **447**, 112 (2007).
[50] Luca Giomi, Tanniemola B. Liverpool, and M. Cristina Marchetti, Sheared active fluids: Thickening, thinning, and vanishing viscosity, Phys. Rev. E **81**, 051908 (2010).
[51] T. B. Liverpool and M. C. Marchetti, Rheology of Active Filament Solutions, Phys. Rev. Lett. **97**, 268101 (2006).
[52] M. Nakamura, L. Chen, S. C. Howes, T. D. Schindler, E. Nogales, and Z. Bryant, Remote control of myosin and kinesin motors using light-activated gearshifting, Nat. Nanotechnol. **9**, 693 (2014).
[53] K. R. S. Kumar, A. S. Amrutha, and N. Tamaoki, Spatiotemporal control of kinesin motor protein by photoswitches enabling selective single microtubule regulations, Lab Chip **16**, 4702 (2016).